3926 *Chem. Mater.* **2010,** *22,* 3926–3932
DOI:10.1021/cm1002737

CHEMISTRY OF MATERIALS
Article

Synthesis and Application of 1,3,4,5,7,8-Hexafluorotetracyanonaphthoquinodimethane (F6-TNAP): A Conductivity Dopant for Organic Light-Emitting Devices

Phillip K. Koech, Asanga B. Padmaperuma,* Liang Wang, James S. Swensen, Evgueni Polikarpov, Jens T. Darsell, James E. Rainbolt, and Daniel J. Gaspar

Energy and Environment Directorate, Pacific Northwest National Laboratory, Richland, Washington 99352

Received January 27, 2010. Revised Manuscript Received May 18, 2010

Conductivity dopants are used in organic light-emitting devices (OLEDs) to reduce the operating voltage and consequently improve the power efficiency. Here, we report the synthesis, as well as photophysical and electroluminescent properties, of an organic molecular *p*-type conductivity dopant: 1,3,4,5,7,8-hexafluorotetracyanonaphthoquinodimethane (F6-TNAP). F6-TNAP was obtained in a three-step two-pot synthesis from commercially available octafluoronaphthalene. When 1%−5% of F6-TNAP was coevaporated with *N*,*N*′-di-1-naphthyl-*N*,*N*′-diphenyl-1,1′-biphenyl-4,4′diamine (α-NPD) an absorption band at 950 nm was formed, which is attributed to charge transfer and assigned to the F6-TNAP radical anion. Single-carrier (hole-only) devices fabricated with F6-TNAP doped into α-NPD as the hole transport layer (HTL) show a >2 V decrease in operating voltage, compared to the undoped device. A decrease in operating voltage was also demonstrated in blue OLED devices using a F6-TNAP-doped HTL, with only a slight decrease in external quantum efficiency, thus resulting in a net improvement in power efficiency. These results demonstrate that F6-TNAP may be useful in generating high-efficiency OLEDs.

Introduction

Organic light-emitting devices (OLEDs) have been widely studied in the past two decades for use in flat panel displays and more-efficient lighting products.[1] For lighting applications, high external quantum efficiency at low operating voltages and high brightness is required for improved energy utilization. High internal quantum efficiency (IQE) has been achieved by utilizing organometallic phosphorescent emitters doped into host materials, which enable harvesting of both singlet and triplet excitons.[2] Conductivity doping of the charge transporting layers reduces device operating voltages. It has been demonstrated that doping the hole transport and/or the electron transport layers in an OLED improves bulk conductivity and decreases the injection barriers at the interfaces, resulting in lower operating voltage.[3] There are a limited number of *p*-type conductivity dopants (*p*-dopants) suitable for use in organic electronic hole transporting layers (HTLs). Although inorganic oxidants such as I_2,[4] $FeCl_3$,[5] $SbCl_5$,[6] ReO_3,[7] and WO_3[8] have been employed as *p*-dopants; these dopants are highly toxic, require high evaporation temperatures, and generate mobile ions that diffuse or drift at high electric field. These drawbacks severely lower device efficiency and lifetime. A molybdenum tris(dithiolene) complex has recently been reported as a *p*-dopant.[9] Strong organic acceptor compounds such as 2,3,5,6-tetrafluoro-7,7,8,8,-tetracyanoquinodimethane (F4-TCNQ)[10] and its derivative F2-HCNQ[11] have also been exploited as dopants in OLEDs. However, controlling doping concentration during vacuum evaporation and preventing molecular diffusion of dopants through the layers in a device remain a

*Author to whom correspondence should be addressed. Tel.: 509-372-4895. Fax: 509-375-2186. E-mail: asanga.padmaperuma@pnl.gov.

(1) (a) Tang, C. W.; Van Slyke, S. A. *Appl. Phys. Lett.* **1987**, *51*, 913. (b) D'Andrade, B. W.; Forrest, S. R. *Adv. Mater.* **2004**, *16*, 1585. (c) Forrest, S. R. ; Thompson, M. E. Chem. Rev. **2007**, *107*, 923 and references therein.
(2) (a) Baldo, M. A.; O'Brien, D. F.; You, Y.; Shoustikov, A.; Sibley, S.; Thompson, M. E.; Forrest, S. R. *Nature* **1998**, *395*, 151. (b) Baldo, M. A.; Lamansky, S.; Thompson, M. E.; Forrest, S. R. *Appl. Phys. Lett.* **1999**, *75*, 4. (c) Yersin, H. *Top. Curr. Chem.* **2004**, *241*, 1. (d) Kawamura, Y.; Goushi, K.; Brooks, J.; Brown, J. J.; Sasabe, H.; Adachi, C. *Appl. Phys. Lett.* **2005**, *86*, 071104.
(3) Hang, J.; Pfeiffer, M.; Werner, A.; Blochwitz, J.; Leo, K. *Appl. Phys. Lett.* **2002**, *80*, 139.
(4) Huang, F.; MacDiarmid, A. G. *Appl. Phys. Lett.* **1997**, *71*, 2415.
(5) Romero, D. B.; Schaer, M.; Zuppiroli, L. *Appl. Phys. Lett.* **1995**, *67*, 1659.
(6) Ganzorig, C.; Fujirira, M. *Appl. Phys. Lett.* **2000**, *77*, 4212.
(7) Leem, D.-S.; Park, H.-D.; Kand, J.-W.; Lee, J.-H.; Kim, J, W.; Kim, J.-J. *Appl. Phys. Lett.* **2007**, *91*, 011113.
(8) Chang, C.-C.; Hsieh, M.-T.; Chen, J.-F. *Appl. Phys. Lett.* **2006**, *89*, 253504.
(9) (a) Qi, Y.; Sajoto, T.; Barlow, S.; Kim, E.-G.; Brédas, J.-L.; Marder, S. R.; Kahn, A. *J. Am. Chem. Soc.* **2009**, *131*, 12530. (b) Qi, Y.; Sajoto, T.; Kröger, M.; Kandabarow, A. M.; Park, W.; Barlow, S.; Kim, E.-G.; Wielunski, L.; Feldman, L. C.; Bartynski, R. A.; Brédas, J.-L.; Marder, S. R.; Kahn, A. *Chem. Mater.* **2009**, *22*, 524.
(10) (a) Matsushima, T.; Adachi, C. *Appl. Phys. Lett.* **2006**, *89*, 253506. (b) Blochwitz, J.; Pfeiffer, M.; Fritz, T.; Leo, K. *Appl. Phys. Lett.* **1998**, *73*, 729. (c) Zhou, X.; Pfeiffer, M.; Blochwitz, J.; Werner, A.; Nollau, A.; Fritz, T.; Leo, K. *Appl. Phys. Lett.* **2001**, *73*, 3202.
(11) (a) Gao, Z. Q.; Mi, B. X.; Xu, G. Z.; Wan, Y. Q.; Gong, M. L.; Cheah, K. W.; Chen, C. H. *Chem. Commun.* **2008**, 117. (b) Mi, B. X.; Gao, Z. Q.; Cheah, K. W.; Chen, C. H. *Appl. Phys. Lett.* **2009**, *94*, 073507.

Published on Web 06/09/2010

challenge for these molecules because of the high volatility and low sticking coefficient. These problems reinforce the need for development of less-volatile organic *p*-dopants that can be vacuum-processed for organic electronics applications. Herein, we report the synthesis, photophysical, and device characteristics of the *p*-dopant 1,3,4,5,7,8-hexafluorotetracyanonaphthoquinodimethane (F6-TNAP) based on the tetracyanonaphthoquinodimethane (TNAP) core. TNAP has been synthesized[12] and its charge-transfer properties studied.[12a,13] The reduction potential of this molecule is 0.2 V (vs SCE),[14] which is similar that of TCNQ. Thus, similar to TCNQ, the TNAP molecule cannot be used as a *p*-dopant for commonly used hole transporting materials, which require reduction potentials close to 0.5 V. Substitution of the H atoms in TNAP with F atoms yields a reduction potential closer to 0.5 V, allowing for favorable electron transfer. Furthermore, the increased molecular weight renders the F6-TNAP more amenable to vapor deposition than F4-TCNQ. To the best of our knowledge, there are no reports describing the synthesis of this compound in the chemical literature; however, the use of this compound as a conductivity dopant has been reported in the patent literature.[15]

Experimental Details

Synthesis and Characterization. All reactions were run under an atmosphere of argon, unless otherwise indicated. Solvents were transferred via canula or a plastic syringe. Flasks were oven-dried and cooled under vacuum. Anhydrous dimethoxyethane (DME) and octafluoronapthalene were purchased from Aldrich Chemical Co. and used without further purification. *Tert*-butylmalonitrile was purchased from TCI America Chemical Co. and was used as received. Nuclear magnetic resonance (NMR) spectra were obtained using a Varian Oxford 500 MHz spectrometer at the following frequencies: 499.8 MHz (^{1}H), 202.3 MHz (^{31}P), 125.7 MHz (^{13}C), and 470.2 MHz (^{19}F). The chemical shifts are reported in delta (δ) units, parts per million (ppm) downfield from tetramethylsilane or appropriate solvent reference. Coupling constants are reported in Hertz (Hz) for ^{1}H, ^{19}F, and ^{13}C spectra. High-resolution mass spectra (HRMS) were acquired using a LTQ Orbitrap mass spectrometer from Thermo Scientific Company as *m*/*e* (relative intensity). Time-of-flight secondary ion mass spectra (ToF-SIMS) were obtained using a ToF-SIMS V time-of-flight secondary ion mass spectrometer (IONTOF GmbH, Münster, Germany). Elemental analysis was performed by Columbia Analytical Services (Tuscon, AZ). The thermal behavior of F6-TNAP powders was studied with differential scanning calorimetry (DSC) and thermogravimetric analysis (TGA) using a Netzsch simultaneous thermal analyzer (STA 449 Jupiter). Powder samples with a mass of ~5 mg were lightly pressed into the bottom of open aluminum pans and heated at 10 °C/min from 25 °C to 532 °C under N_2 gas at a flow rate of 50 mL/min. The STA 449 Type-K thermocouples were calibrated using gallium, indium, and tin metals, and the sensitivity of the DSC signal was calibrated by heating a sapphire standard.

2-Tert-butyl-2-[6-(1,1-dicyano-2,2-dimethyl-propyl)-1,3,4,5,7,8-hexafluoro-naphthalen-2-yl]-malononitrile (**2**). Sodium hydride (1.62 g, 40.43 mmol, 60% in mineral oil) was charged into a clean dry Schlenk flask, and then anhydrous DME 10 mL was added. The resulting suspension was cooled to 0 °C, and then a solution of *t*-butylmalononitrile (4.71 g, 38.59 mmol) in 10 mL of DME was added dropwise. The reaction mixture was allowed to warm to room temperature, and stirring was continued at this temperature for 30 min. Octafluoronapthalene (5 g, 18.37 mmol) in 10 mL of DME was added to the resulting homogeneous solution. When the addition was complete, the reaction was heated at reflux for 18 h. The reaction mixture was allowed to cool to room temperature and then quenched with water (100 mL), whereupon a brown precipitate formed. The precipitate was filtered and rinsed with water (2 × 50 mL) and diethyl ether (3 × 30 mL). The resulting off-white solid was dried under vacuum to give intermediate 2 (6.70 g, 14.5 mmol) in 79% yield. ^{1}H NMR (500 MHz, DMSO-d_6) δ (ppm): 1.29 (s, 18H). ^{19}F NMR (470 MHz, DMSO-d_6) δ (ppm, referenced to C_6F_6 at −164.9 ppm): −113.2 (dd, J_{F-F} = 73.2, 18.3 Hz, 1F), −133.8 (d, J_{F-F} = 18.3 Hz, 1F), −147.2 (d, J_{F-F} = 76.3 Hz, 1F). HRMS (ESI): calculated [M+Na] for $C_{24}H_{18}F_6N_4Na$, *m*/*z* = 499.1300; found, *m*/*z* = 499.1331.

1,3,4,5,7,8-Hexafluorotetracyanonaphthoquinodimethane (*F6-TNAP*). To a refluxing solution of diphenyl ether (150 mL) was added 2-*tert*-butyl-2-[6-(1,1-dicyano-2,2-dimethyl-propyl)-1,3,4,5,7,8-hexafluoro-naphthalen-2-yl]-malononitrile (**2**) (5.0 g, 10.84 mmol) as a solid in one portion; vigorous gas evolution was observed instantly. The reaction was refluxed for 5 min, and then the heat source was removed to allow air cooling to 195 °C. The reaction mixture was then immersed in a water bath until the temperature reached 40 °C. At this point, 150 mL of diethyl ether were added followed by 150 mL of 4% sodium bicarbonate. The aqueous phase was separated and the organic phase was extracted with 2% $NaHCO_3$ solution (2 × 70 mL). The combined bicarbonate fraction was filtered, and the filtrate was acidified to pH 1.0, using concentrated HCl to form a white precipitate. To this suspension, bromine water was added until the brownish color persisted, at which point the precipitate turned purple. This precipitate was collected by filtration and then washed with water until the washing reached pH ~7.0. The purple solid was washed with diethyl ether (30 mL) and then dried under vacuum to give (2.7 g, 7.45 mmol) 69% yield of F6-TNAP. ^{19}F NMR (470 MHz, Tol-d_8) δ (ppm, referenced to C_6F_6 at −164.9 ppm): −103.5 (d, J_{F-F} = 79.4 Hz, 1F), −137.1 (m, 2F). MS (ToF-SIMS) *m*/*z* 362.02 (calcd *m*/*z* 362.00). Anal. Calcd for $C_{16}F_6N_4$: C, 53.06; N, 15.47; Found: C, 53.10%; N, 15.96%.

(12) (a) Diekmann, J.; Hertler, W. R.; Benson, R. E.J. Org. Chem. **1963**, *28*, 2719. (b) Sandman, D. J.; Garito, A. F. *J. Org. Chem.* **1974**, *39*, 1165.
(13) (a) Yamaguchi, S.; Potember, R. S. *Synth. Met.* **1996**, *78*, 117. (b) Ostapenko, N. I.; Sekirin, I. V.; Tulchynskaya, D. N.; Suto, S.; Watanabe, A. *Synth. Met.* **2002**, *129*, 19.
(14) Wheland, R. C.; Gillson, J. L. *J. Am. Chem. Soc.* **1976**, *98*, 3916.
(15) (a) Zeika, O.; Birnstock, J.; Limmert, M.; Vehse, M. (Novaled AG, Germany). Eur. Patent Application EP1912268 A1 20080416, 2008. (b) Hofmann, M.; Birnstock, J.; Blochwitz, N. J.; Werner, A.; Pfeiffer, M.; Harada, K. (Novaled AG, Germany). Eur. Patent Application EP19122681713136 A1 20061018, 2006; 26 pp.
(16) Bylaska, E. J.; de Jong, W. A.; Govind, N.; Kowalski, K.; Straatsma, T. P.; Valiev, M.; Wang, D.; Apra, E.; Windus, T. L.; Hammond, J.; Nichols, P.; Hirata, S.; Hackler, M. T.; Zhao, Y.; Fan, P.-D.; Harrison, R. J.; Dupuis, M.; Smith, D. M. A.; Nieplocha, J.; Tipparaju, V.; Krishnan, M.; Wu, Q.; T. Van Voorhis, Auer, A. A.; Nooijen, M.; ,Crosby, L. D.; Brown, E.; Cisneros, G.; Fann, G. I.; Fruchtl, H.; Garza, J.; Hirao, K.; Kendall, R.; Nichols, J. A.; Tsemekhman, K.; Wolinski, K.; Anchell, J.; Bernholdt, D.; Borowski, P.; Clark, T.; Clerc, D.; Dachsel, H.; Deegan, M.; Dyall, K.; Elwood, D.; Glendening, E.; Gutowski, M.; Hess, A.; Jaffe, J.; Johnson, B.; Ju, J.; Kobayashi, R.; Kutteh, R.; Lin, Z.; Littlefield, R.; Long, X.; Meng, B.; Nakajima, T.; Niu, S.; Pollack, L.; Rosing, M.; Sandrone, G.; Stave, M.; Taylor, H.; Thomas, G.; van Lenthe, J.; Wong, A.; Zhang, Z. NWChem, A Computational Chemistry Package for Parallel Computer, Version 5.1; Pacific Northwest National Laboratory, Richland, WA, **2007**.

Scheme 1. Synthesis of F6-TNAP

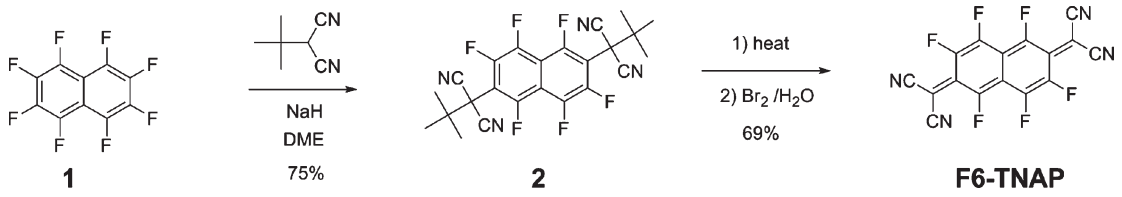

Theoretical Calculations. All calculations were performed using the NWChem computational package[16] at the Molecular Science Computing Facility at the Environmental Molecular Science Laboratory. Molecular orbitals and bond lengths were visualized using the Extensible Computational Chemistry Environment (ECCE),[17] which is a component of the Molecular Science Software Suite (MS^3) developed at Pacific Northwest National Laboratory.

Electrochemical Measurements. Conducted using a Princeton Applied Research model 263A potentiostat with a Ag/AgCl reference electrode, a platinum wire as the counter electrode, and glassy carbon as the working electrode (scan speeds of 20−300 mV/s). The potentials were measured in dichloromethane distilled over CaH_2. Tetrabutylammonium hexafluorophosphate was used as a supporting electrolyte. UV−visible absorption spectra were collected on a Varian Cary 5 UV−vis-NIR spectrophotometer. Lowest unoccupied molecular orbital (LUMO) energy levels were estimated from solution electrochemical reduction potentials. Highest occupied molecular orbital (HOMO) levels were estimated from electrochemical oxidation potentials or the optical band gap where electrochemical measurements were not feasible.

OLED Fabrication and Testing. Commercial ITO substrates (Colorado Concept Coatings, 15 Ω/sq) were cleaned by a sequential series of solvents, including a dilute Tergitol solution, deionized water, trichloroethane, acetone, and 2-propanol with sonication. The substrates were dried with flowing nitrogen. As a final cleaning step before use, the substrates were treated with UV ozone for 10 min. The substrates were then loaded into a nitrogen glovebox (< 1 ppm H_2O, < 0.5 ppm O_2) coupled to a multichamber vacuum deposition system. Organic layers were sequentially deposited onto the ITO substrates by thermal evaporation from Ta boats in a high-vacuum chamber with base pressure below 3×10^{-7} Torr. Cathodes were defined by thermally depositing a 1-nm-thick layer of LiF, immediately followed by a 100-nm-thick layer of aluminum through a shadow mask with 1-mm-diameter circular openings. A quartz crystal oscillator placed near the substrate was used to monitor the thicknesses of the films, which were calibrated ex situ using ellipsometry. The deposited stack of organic and metal layers is depicted as ITO/350 Å *x*% F6TNAP:α-NPD/50 Å TCTA/150 Å 6% FIrpic:mCP/500 Å PO15/10 Å LiF/1000 Å Al, where *x*% = 0%, 1%, 2%. Here, the F6-TNAP doped (*x*%) *N*,*N*′-di-1-naphthyl-*N*,*N*′-diphenyl-1,1′-biphenyl-4,4′diamine (α-NPD) constitutes the hole-transporting layer (HTL). The emissive layer (EML) is composed of host 3,5′-*N*,*N*′-dicarbazole-benzene (mCP) doped with a blue phosphor iridium(III) bis[(4,6-difluorophenyl)-pyridinato-N,C2′]picolinate (FIrpic), and 2,8-bis(diphenylphosphoryl)dibenzothiophene (PO15) functions as a hole-blocking/electron-transporting layer (ETL). Devices were tested in air with electrical contact made using a tungsten probe tip on the ITO anode and a 0.002-in.-diameter gold wire directly probing the aluminum cathode. Current−voltage characteristics were measured with an Agilent Technologies Model 4155B semiconductor parameter analyzer. Light output was detected using a 1 cm^2 Si photodetector placed behind the OLED, and device brightness was directly measured using a Konika-Minolta Chromameter CS-200. No corrections were made for light waveguided in the organic thin films or the substrate. EL spectra were recorded with an Acton Research Corporation (ARC) Spectrum model CCD detector on an ARC Spectra Model 150 dual grating monochromator.

Results and Discussion

Synthesis. Synthesis of F6-TNAP starts with nucleophilic aromatic substitution on commercially available octafluoronaphthalene using the sodium anion of *t*-butylmalononitrile to furnish 2-*tert*-butyl-2-[6-(1,1-dicyano-2,2-dimethyl-propyl)-1,3,4,5,7,8-hexafluoro-naphthalen-2-yl]-malononitrile **2** (see Scheme 1). Compound **2** was converted to F6-TNAP by refluxing in diphenyl ether to remove the *t*-butyl groups, followed by acidification of the incipient dianion, which is then treated with bromine water to provide F6-TNAP as chemically pure material, according to ^{19}F NMR analysis.

Thermal Studies. F6-TNAP was purified by gradient sublimation under high vacuum in a Teflon-lined ceramic boat placed in a Teflon-lined glass tube to prevent undesired chemical reactions from occurring between F6-TNAP and the glass at elevated temperature.[18] F6-TNAP sublimes at 220−260 °C, which is significantly higher that of F4-TCNQ, which has a sublimation temperature of 135−145 °C under high vacuum (10^{-6} Torr). After sublimation, two forms of the product were isolated, in the form of purple plates and green crystals, possessing identical ^{19}F NMR and UV−vis absorption spectra. The purple plates were collected at the cooler zone of the furnace below 250 °C and the green crystals at the zone above 260 °C. This indicates a possible phase change in the 250−260 °C range. This phenomenon has been observed in the literature for TNAP, where a purple black solid transforms to a lavender solid upon heating above 155 °C.[18] This report presumes that the lavender material of TNAP is a polymeric form.

DSC analysis was conducted on both purple and green fractions of F6-TNAP. Results are shown in Figure 1a. The purple sample exhibits an exotherm between 240 °C and 270 °C that is not seen in the green sample. We attribute this exotherm to a phase change from the purple

(17) Black, G.; Daily, J.; Didier, B.; Elsethagen, T.; Feller, D.; Gracio, D.; Hackler, M.; Havre, S.; Jones, D.; Jurrus, E.; Keller, T.; Lansing, C.; Matsumoto, S.; Palmer, B.; Peterson, M.; Schuchardt, K.; Stephan, E.; Sun, L.; Swanson, K.; Taylor, H.; Thomas, G.; Vorpagel, E.; Windus, T.; Winters, C. ECCE, A Problem Solving Environment for Computational Chemistry, Software Version 4.5.1; Pacific Northwest National Laboratory, Richland, WA, **2007**.

(18) McGhie, A. R.; Garito, A. F.; Heeger, A. J. *J. Cryst. Growth* **1974**, *22*, 295.

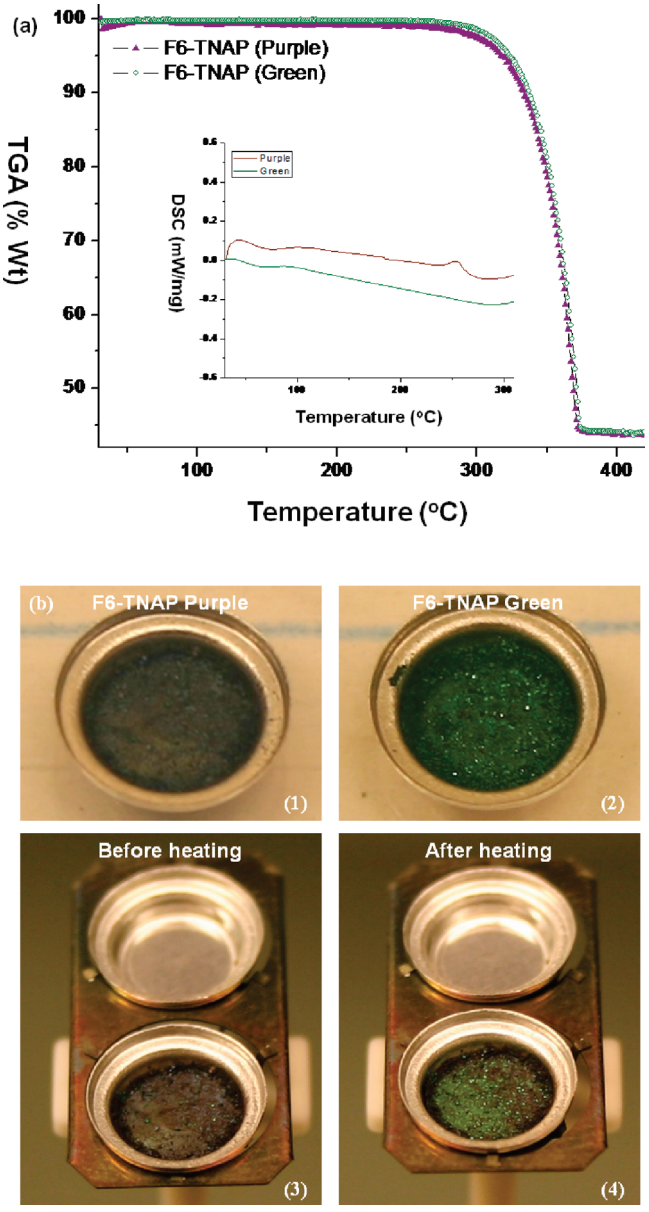

Figure 1. (a) TGA/DSC analysis of green and purple forms of F6-TNAP. (b) Pictures of purple and green F6-TNAP (1, purple form; 2, green form; 3, purple form prior to heating; and 4, purple form after heating to 280 °C under a nitrogen environment.

form to the green form. The TGA analysis confirms that F6-TNAP does not exhibit weight loss upon heating up to 280 °C, at which temperature decomposition occurs. No significant differences were observed between the mass-loss behaviors of the green and purple versions of F6-TNAP. Figure 1b shows both green and purple F6-TNAP before and after heating at 280 °C. As expected, most of the purple sample had turned green, whereas the green sample did not change color. Our experimental data (see the Supporting Information) indicates that the different colors of these two crystals are unlikely to be due to impurities, because no difference was found in the performance of devices using F6-TNAP sublimed from these two crystal sources. Therefore, we speculate that these materials are chemically identical but differ in the morphology or molecular packing, which exists in two different phases, at low and high temperatures, showing purple and green colors, respectively. Despite the morphological differences of the green and purple F6-TNAP, single-carrier and OLED devices fabricated from either source exhibited identical performance.

Electronic Properties. The geometries of F4-TCNQ and F6-TNAP were optimized at the B3LYP/cc-PVTz level. The energy of the HOMO and LUMO levels were calculated from the optimized structures and are summarized in Table 1. The HOMO and LUMO energies of F6-TNAP are predicted to be −7.48 eV and −5.57 eV, respectively. The E_{LUMO} of the F6-TNAP is close to that of F4-TCNQ, whereas the HOMO energy of F6-TNAP is shallower than that of F4-TCNQ, which results in a narrower bandgap for the former. Excitation energies of the singlet states were calculated using the time-dependent DFT method (TD-DFT) utilizing the B3LYP functional with the cc-PVTz basis set. The lowest energy absorbance bands of both molecules are due to the $S_1 \leftarrow S_0$ transition. The energies of the first nonzero singlet excitation for F6-TNAP and F4-TCNQ are 1.92 and 2.45 eV, respectively. Thus, the TD-DFT studies predict a 0.52 eV red shift in absorbance for F6-TNAP, compared to F4-TCNQ.

The solution absorbance spectrum of F6-TNAP was measured in CH_2Cl_2 (1×10^{-5} M) and compared to that of F4-TCNQ (Figure 2). The absorbance spectrum of F6-TCNQ is slightly broader and, as predicted by TD-DFT studies, the absorbance maximum is red-shifted by 89 nm (0.59 eV), compared to that of F4-TCNQ. The optical bandgap of the molecules were estimated from the absorbance spectra and are shown in Table 1.

Based on CV data and optical bandgap data, the lowest unoccupied molecular orbital (LUMO) and the highest occupied molecular orbital (HOMO) energy levels can be estimated. $E_{LUMO} = E_{ref} - E_{red}$, where E_{ref} is the potential of the reference, relative to the vacuum level (for Ag/AgCl, −4.72 eV),[19] and E_{red} is the potential of the first reduction peak extracted directly from the CV data. Kahn reported a value of $E_{LUMO} = -5.24$ eV for F4-TCNQ, using inverse photoelectron spectroscopy (IPES),[20] which is consistent with the E_{LUMO} value estimated from CV data by Gao and co-workers.[11] Based on the reduction potential measured for F6-TNAP (see Figure 3), it is predicted to have a value of E_{LUMO} of −5.37 eV, which is similar to but slightly deeper than that of F4-TCNQ. For effective doping, the LUMO of the dopant should be slightly lower in energy than the HOMO of the donor or host material. From our results, it is apparent that HTL materials for which F4-TCNQ is a suitable conductivity dopant can also be used as hosts with F6-TNAP.

(19) (a) Andersson, M. R.; Berggren, M.; Inganäs, O.; Gustafsson, G.; Gustafsson-Carlberg, J. C.; Selse, D.; Hjertberg, T.; Wennerström, O. *Macromolecules* **1995**, *28*, 7525. (b) Agrawal, A. K; Jenekhe, S. A. *Chem. Mater.* **1996**, *8*, 579. (c) Seguy, I.; Jolinat, P.; Destruel, P.; Farenc, J.; Mamy, R.; Bock, H.; Ip, J.; Nguyen, T. P. *J. Appl. Phys.* **2001**, *89*, 5442. (d) D'Andrade, B. W.; Datta, S.; Forrest, S. R.; Djurovich, P.; Polikarpov, E.; Thompson, M. E. *Org. Electron.* **2005**, *6*, 11.
(20) Gao, W.; Kahn, A. *Appl. Phys. Lett.* **2001**, *79*, 4040.

Table 1. Absorbance Properties, Reduction Potentials (from CV), and Measured and Theoretically Predicted HOMO and LUMO Energies for F4-TCNQ and F6-TNAP

	Solution Absorbance		Solution Electrochemistry			Theory	
material	λ_{max} (nm)	E_g (eV)	$E_{1/2}^{red}$ (V)[a]	E_{LUMO} (eV)[b]	E_{HOMO} (eV)[c]	E_{LUMO} (eV)[d]	E_{HOMO} (eV)[d]
F6-TNAP	481	2.44	0.65	−5.37	−7.81	−5.57	−7.48
F4-TCNQ	392	2.98	0.63	−5.35	−8.33	−5.51	−7.96

[a] First half-electron reduction potential in CH_2Cl_2, with respect to a Ag/AgCl electrode. [b] Estimated from solution electrochemistry data using the following equation: $E_{LUMO} = -4.72 - E_{red}$. [c] Estimated from solution electrochemistry data and the optical gap using the following equation: $E_{HOMO} = E_{LUMO} + E_g$. The measured potential for Fc/Fc+ in DCM vs Ag/AgCl electrode is +0.44 V. [d] *NWChem* theoretical gas phase prediction.

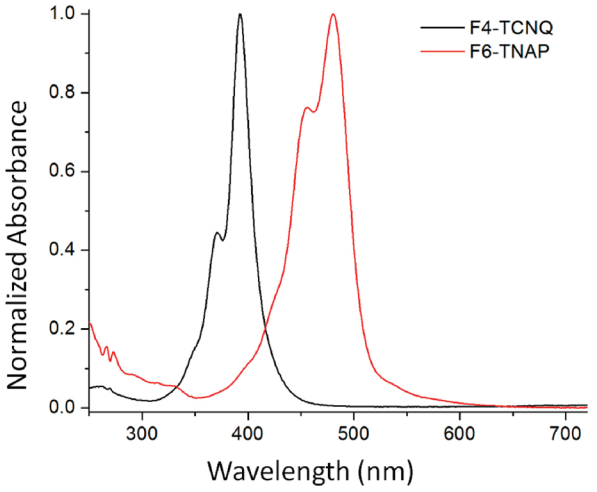

Figure 2. Solution absorbance spectra for F6-TNAP and F4-TCNQ.

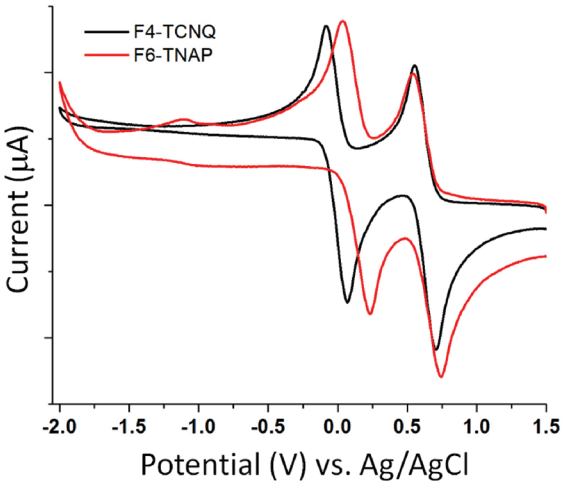

Figure 3. Cyclic voltammetry of F4-TCNQ (black trace) and F6-TNAP (red trace).

Absorbance Studies of the Host−Dopant Interaction. The UV−vis absorption spectra of undoped *N*,*N*′-di-1-naphthyl-*N*,*N*′-diphenyl-1,1′-biphenyl-4,4′diamine (α-NPD, 35 nm) and F6-TNAP-doped α-NPD (1% to 5%, 35 nm) films deposited on quartz are shown in Figure 4. The absorption spectrum of undoped α-NPD shows a strong absorption peak centered at 350 nm, while doping with F6-TNAP reveals additional absorption peaks at 475 and 950 nm, the intensity of which increases with the amount of F6-TNAP. The peak at 350 nm is due to the π,π^* transition of α-NPD. These observations are similar to those seen when doping α-NPD with ReO_3[7] or F4-TCNQ. The absorption peak at 475 nm is due to the π,π^* transition of α-NPD$^{\bullet+}$ which could be superimposed with F6-TNAP.[9] The near-IR absorption peak at ∼950 nm is attributed to the F6-TNAP$^{\bullet-}$. This radical anion was assigned by reducing F6-TNAP in solution with ferrocene, which gave two near-IR absorption peaks at 970 and 1150 nm (see the Supporting Information). Although the intensity of the absorption band in the near IR is most evident at doping levels beyond 5%, there is evidence of charge transfer, even at lower doping levels. The charge transfer occurs when electrons are donated from the HOMO of α-NPD to the LUMO of F6-TNAP, leaving a mobile charge carrier (hole) on the hole transport material α-NPD. Therefore, the hole density in the hole transport layer is expected to increase upon doping with F6-TNAP. This should improve hole transport through the NPD layer within an OLED structure and thereby reduce the operating voltage of the OLED device.

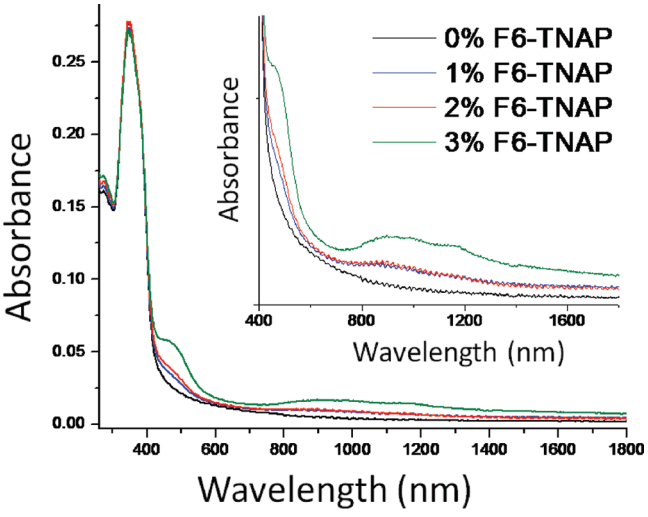

Figure 4. UV−vis absorption spectra of undoped α-NPD and *X*% F6-TNAP-doped α-NPD films deposited on a quartz substrate.

Single-Carrier Device Studies. To further evaluate the hole injection and transport characteristics of the α-NPD/F6-TNAP system, hole-only devices were fabricated. The *J*−*V* characteristics of the hole-only devices are shown in Figure 5. Three device architectures were tested. A control device (ITO/undoped α-NPD (150 nm)/Au (10 nm)/Al (150 nm)), a bulk conductivity-doped device (ITO/α-NPD:1.5% F6-TNAP (150 nm)/Au (10 nm)/Al (150 nm)), and an interface conductivity-doped device (ITO/α-NPD:1.5% F6-TNAP (5 nm)/α-NPD (145 nm)/Au (10 nm)/Al (150 nm)) were also

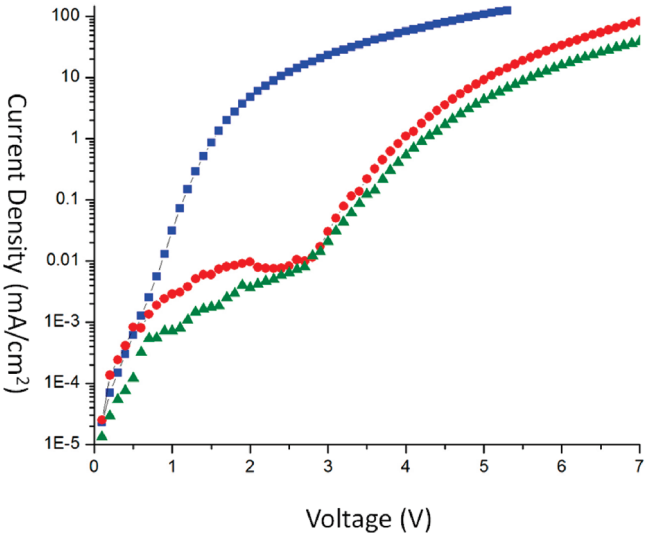

Figure 5. Plot of the $J-V$ characteristics of the hole-only devices for device structures: ITO/1.5% F6-TNAP:α-NPD (150 nm)/Au (10 nm)/Al (150 nm) (blue squares); ITO/1.5% F6-TNAP:α-NPD (5 nm)/α-NPD (145 nm)/Au (10 nm)/Al (150 nm) (red circles); and ITO/α-NPD (150 nm)/Au (10 nm)/Al (150 nm) (green triangles).

fabricated and studied. The undoped device demonstrates typical charge transport behavior for an organic thin film. Upon bulk doping (the blue line), the conductivity of the device significantly improved with a corresponding decrease in the operating voltage. In the interface-doped devices (the red line), no such improvement to the conductivity or a reduction of the voltage was observed; the $J-V$ properties were similar to that of the undoped (the green line) devices. Bulk conductivity doping gave the largest decrease in operating voltage, compared to interface doping. This data indicates doping α-NPD with F6-TNAP enhances transport in the HTL due to the increase of charge carrier (hole) concentration. The hole-only device with α-NPD:1.5% F6-TNAP/undoped α-NPD layers follows similar behavior to that of the device with the undoped α-NPD layer, indicating that the primary contribution of F6-TNAP is to increase the bulk conductivity of α-NPD, rather than just modifying the anode/HTL interface for better charge injection. A similar enhancement of α-NPD bulk conductivity by *p*-doping with F4-TCNQ has been shown by other researchers.[21]

Blue OLED Studies. To demonstrate improvement in OLED power efficiency, the F6-TNAP/α-NPD system was used as the HTL in a blue OLED. The emissive layer (EML) consisted of the host 3,5′-*N*,*N*′-dicarbazole-benzene (mCP) doped with the blue phosphor iridium(III) bis[(4,6-difluorophenyl)-pyridinato-N,C2′]picolinate (FIrpic). A wide bandgap material, 2,8-bis(diphenylphosphoryl)-dibenzothiophene (PO15), which was developed in our laboratories, was used as the hole blocking/electron-transporting layer (HBL/ETL). The device studied had the following structure: ITO/x% F6TNAP:α-NPD (35 nm)/TCTA (5 nm)/6% FIrpic:mCP (15 nm)/PO15 (50 nm)/LiF (1 nm)/Al (100 nm), where x% is 0 and 2 wt % F6-TNAP doped into the α-NPD HTL. The effects of doping on the drive voltage, external quantum efficiency (EQE), and power efficiency for these OLEDs are shown in Figure 6.

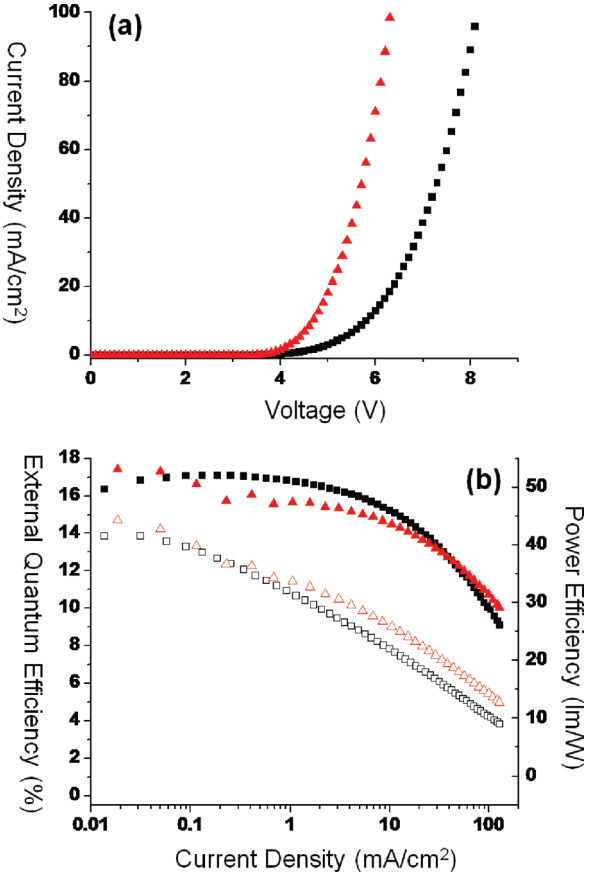

Figure 6. (a) Current density as a function of voltage and (b) external quantum efficiency (EQE) (denoted by solid symbols) and power efficiency (denoted by hollow symbols) as a function of current density for blue OLEDs with the following device structure: ITO/x% F6-TNAP: α-NPD (35 nm)/TCTA (5 nm)/6% FIrpic:mCP (15 nm)/PO15 (50 nm)/LiF (1 nm)/Al (100 nm), where x = 0% (black squares) and 2% (red triangles) F6-TNAP doped into the α-NPD HTL.

The $J-V$ characteristics for the devices are shown in Figure 6a. There is a clear reduction in drive voltage upon doping α-NPD with 2 wt % F6-TNAP, which is consistent with increased conductivity of α-NPD upon doping with F6-TNAP, as demonstrated in Figure 5. At a current density of 10 mA/cm^2, the undoped device has an operating voltage of 5.8 V, whereas upon doping α-NPD with 2 wt % F6-TNAP, the voltage reduces to 4.6 V. This decrease in the operating voltage is attributed to the formation of a charge-transfer complex between F6-TNAP and α-NPD and the consequent increase of hole density within HTL.

There is a slight reduction in EQE when the HTL is doped with F6-TNAP, as seen in Figure 6b. Absorption of the FIrpic electroluminescence by F6-TNAP is one possible explanation for this observation, since the absorption spectra of F6-TNAP overlaps with the emission spectra of FIrpic. However, at lower doping concentrations (< 2%), the absorption by F6-TNAP should have a negligible effect on the brightness of the device. If the concentration is increased to > 5%, then the absorption by F6-TNAP becomes more significant. Since we use the

(21) (a) Gao, W.; Kahn, A. *J. Appl. Phys.* **2003**, *94*, 359. (b) Gao, W.; Kahn, A. *J. Phys.: Condens. Matter* **2003**, *15*, S2757.

p-dopant at very low concentrations, absorption is not expected to be an issue. We observe that the EQE loss upon doping varies with current density, which indicates the decrease in EQE is more likely due to imperfect charge balance (i.e., an equal number of holes and electrons in the emissive region) in the emissive layer, given the larger hole conduction caused by increased hole conductivity. Despite the slight reduction in EQE, Figure 6b shows that the power efficiency of the F6-TNAP-doped devices is better than that of the undoped devices. Thus, we have reported that conductivity doping of NPD with F6-TNAP leads to increased power efficiency in blue phosphorescent OLEDs.

Conclusion

We have reported the synthesis and chemical, photophysical, and electrochemical properties of 1,3,4,5,7,8-hexafluorotetracyanonaphthoquinodimethane (F6-TNAP). We have demonstrated that doping F6-TNAP into a hole transport layer (HTL) can significantly reduce the operating voltage in both hole-only devices and organic light-emitting devices (OLEDs). This is the first time that F6-TNAP has been demonstrated as a conductivity dopant in a blue OLED. In combination with its simple, low-cost, and easy-to-scale-up synthesis, F6-TNAP has the potential to improve OLED performance. Therefore, the use of conductivity doping is a promising approach in the push to develop OLEDs that reach the power efficiency goals for solid-state lighting. Future research will focus on fabricating and testing *p-i-n* devices, using F6-TNAP as the *p*-dopant, in combination with an *n*-dopant in the electron transport layer (ETL). This approach should enhance charge balance (external quantum efficiency, EQE) and further reduce the drive voltages, leading to optimal power efficiency in blue phosphorescent OLEDs.

Acknowledgment. This project was funded by the Solid State Lighting Program of the U.S. Department of Energy (US DOE), within the Building Technologies Program (BT) (Award No. M6743231, managed by the National Energy Technology Laboratory (NETL)). A portion of this research was performed using EMSL, which is a national scientific user facility sponsored by the Department of Energy's Office of Biological and Environmental Research and is located at Pacific Northwest National Laboratory (PNNL). Computations were performed using *NWChem*, A Computational Chemistry Package for Parallel Computers, Version 5.1 (2007), which was developed at the High Performance Computational Chemistry Group, PNNL, Richland, WA. PNNL is operated by Battelle Memorial Institute for the U.S. DOE (under Contract DE_AC06-76RLO 1830). The authors would like to thank Dr. Rui Zhang and Dr. Zihua Zhu for performing the electrospray ionization mass spectrometry and time-of-flight secondary ion mass spectrometry analyses, respectively.

Supporting Information Available: ^{1}H, ^{19}F NMR spectra for both compound **2** and F6-TNAP (purple and green); UV−vis absorption spectra for both purple and green F6-TNAP, and the blue OLED data. UV−vis absorption spectra for the reduced form of F6-TNAP in solution with ferrocene. (PDF) This material is available free of charge via the Internet at http://pubs.acs.org.